Review Article

Review and Selection Strategy for High-Accuracy Modeling of PWM Converters in DCM

Yu-Jun Mao,[1] Chi-Seng Lam (ID),[1] Sai-Weng Sin,[1,2] Man-Chung Wong,[1,2] and Rui Paulo Martins (ID)[1,2,3]

[1]*State Key Laboratory of Analog and Mixed-Signal VLSI, University of Macau, Macau 999078, China*
[2]*Department of Electrical and Computer Engineering, Faculty of Science and Technology, University of Macau, Macau 999078, China*
[3]*On Leave from Instituto Superior Técnico, Universidade de Lisboa, Lisbon 1649-004, Portugal*

Correspondence should be addressed to Chi-Seng Lam; cslam@umac.mo

Among various modeling methods for DC-DC converters introduced in the past two decades, the state-space averaging (SSA) and the circuit averaging (CA) are the most general and popular exhibiting high accuracy. However, their deduction approaches are not entirely equivalent since they incorporate different averaging processes, thus yielding different small signal transfer functions even under identical operating conditions. Some research studies claimed that the improved SSA can obtain the highest accuracy among all the modeling methods, but this paper discovers and clearly verifies that this is not the case. In this paper, we first review and study these two modeling methods for various DC-DC converters operating in the discontinuous conduction mode (DCM). We also streamline the general model-deriving processes for DC-DC converters, and test and compare the accuracy of these two methods under various conditions. Finally, we provide a selection strategy for a high-accuracy modeling method for different DC-DC converters operating in DCM and verified by simulations, which revealed necessary and beneficial for designing a more accurate DCM closed-loop controller for DC-DC converters, thus achieving better stability and transient response.

1. Introduction

A PWM DC-DC converter operates either in the continuous conduction mode (CCM) or in the discontinuous conduction mode (DCM). For small inductances or light loads, DCM operation is occasionally unavoidable in DC-DC converters, their design being intentionally in DCM to reduce both the inductor's size and the switching frequency. Then, it is necessary to develop a modeling analysis for the DC-DC converter operation in DCM to design a closed-loop controller. In previous works [1–22], various small signal modeling methods of PWM DC-DC converters in CCM and DCM are proposed, where different modeling methods provide either an analytical equation or an equivalent circuit and can be categorized as reduced-order or full-order models, as summarized in Table 1.

Among these small signal modeling methods, the improved state-space averaging (SSA) and the circuit averaging (CA) are the latest to present, with high accuracy, an analytical equation, and an equivalent circuit, respectively. The improved SSA method [6] claims that it has the highest accuracy among all the other modeling methods and can be applied to any circuit composed by inductors and capacitors. But, this conclusion is only proven and verified in a boost converter under specific operating conditions [6]. Besides, this may not hold in other DC-DC converters and under different operating conditions. Moreover, Zeng et al. [13] used the CA method from [5] to deduce the small signal model of a KY converter, but when applying the improved

TABLE 1: Summary of small signal modeling methods.

Method name	Order	Model type
Conventional state-space averaging (SSA) [1]	Reduced order (low accuracy)	Analytical equation
Converter cell [2]	Reduced order (low accuracy)	Equivalent circuit
Full-order SSA [3, 8, 11, 12, 20]	Full order (high accuracy)	Analytical equation
Circuit averaging (CA) [4, 5, 8–10, 13, 14, 17–19, 21, 22]	Full order (high accuracy)	Equivalent circuit
Improved SSA [6, 7, 15, 16]	Full order (high accuracy)	Analytical equation

SSA method to the same case, the CA method yields a better modeling accuracy under some conditions that are discussed in this paper. Contradictions met in CA and SSA methods motivate further analysis and retesting their accuracy in various DC-DC converters under different operating conditions in DCM, in order to derive a selection criterion that allows higher accuracy in the small signal modeling method.

Also, the rather complicated (and not general) original derivation processes of the CA and the improved SSA methods, in which the whole small signal model derivation process should be repeated whenever the DC-DC circuit topology changes, whenever the DC-DC circuit topology changes, leads to unnecessary and time-consuming efforts. Then, another motivation for this paper is to generalize the whole derivation process to attain a general and intuitive model-deriving solution.

The main contributions of this paper are as follows:

(1) To propose and deduct a general and intuitive derivation process of the improved SSA and CA modeling methods for different DC-DC converters, such that their corresponding DCM small signal models can be easily determined.

(2) To study, retest, and compare, through simulations, the accuracy of the improved SSA and CA modeling methods for various DC-DC converters under different operating conditions. Since most of the previous works are either based on the improved SSA or CA, they lack a detailed comparison among them.

(3) To propose a selection strategy of the DCM small signal modeling method in order to obtain high accuracy for different DC-DC converters under different operating conditions.

This paper contributes significantly to the design of a stable and fast transient response DCM closed-loop controller for different DC-DC converters. Section 2 presents the DC analysis of different DC-DC converters in DCM. Section 3 introduces two small signal relationship calculation methods based on the large-signal equation. Section 4 discusses the general DCM large-signal and small signal modeling deduction based on the improved SSA method applied to different DC-DC converters. Then, Section 5 determines the general DCM large-signal and small signal modeling deduction based on the CA method. Section 6 compares the simulation results of the small signal modeling obtained through the improved SSA and the CA methods. Section 7 presents a selection strategy of the DCM small

signal modeling for different DC-DC converters. Finally, the conclusions are drawn in Section 8.

2. DC Analysis of DC-DC Converters in DCM

In the discussion hereafter, if we use the capital letter X to denote the averaged value of a specific variable in one switching frequency (DC value), then the lowercase letter x denotes its large-signal value and $\hat{x}$ denotes its small signal value. The relationship between these three variables is [10]

$$x = X + \hat{x}. \tag{1}$$

2.1. DCM Operation. The DCM operation of the DC-DC converters consists of three intervals. Here, we use D_1, D_2, and D_3 to denote the duty ratio of each interval, respectively, and T_s denotes the switching period. Figure 1 shows the inductor current, i_L, waveform of the DC-DC converters operating in DCM [10].

For a typical DC-DC converter, i_L starts to rise during the charging of the inductor L and begins to drop while the L is discharging. In this paper, we use V_{on} (charging) and V_{off} (discharging) to denote the voltage across the L in the first and the second intervals, respectively. From Figure 1, we can obtain

$$I_{pk} = \frac{V_{on}}{L} D_1 T_s, \tag{2}$$

where I_{pk} denotes the peak value of inductor current i_L, D_1 denotes the duty ratio of charging interval, and T_s denotes the switching period. From Figure 1, the relationship between the peak value (I_{pk}) and average value (I_L) of the inductor current can be expressed as

$$\frac{1}{2} I_{pk} (D_1 + D_2) T_s = I_L T_s, \tag{3}$$

where I_L denotes the average value of the inductor current i_L while T_s and D_2 denotes the duty ratio of the discharging interval. From Figure 1,

$$\frac{V_{on}}{L} D_1 T_s = \frac{-V_{off}}{L} D_2 T_s = I_{pk}. \tag{4}$$

Equation (4) yields the following

$$D_2 = -\frac{V_{on}}{V_{off}} D_1, \tag{5}$$

where V_{on} (charging) and V_{off} (discharging) denote the voltage across the L in the first and the second intervals,
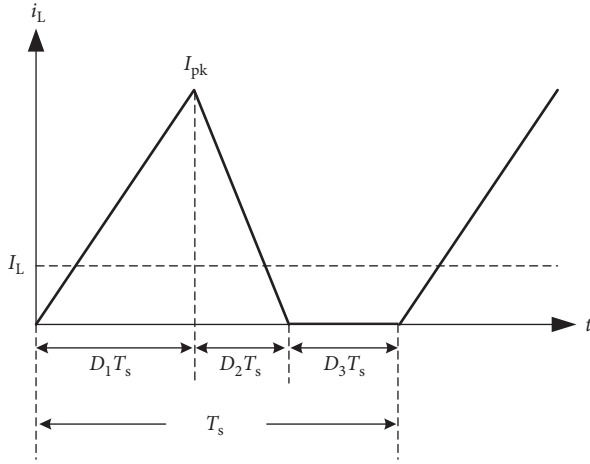
FIGURE 1: Inductor current of DC-DC converters operating in DCM.

respectively. Considering (2), (3), and (5), I_L can be expressed as

$$I_L = \frac{D_1^2 T_s V_{on} (V_{off} - V_{on})}{2L V_{off}}. \tag{6}$$

2.2. DC Parameters Calculation for Different DC-DC Converters in DCM. Before we derive the small signal model, some DC parameters of the circuit operating in DCM need to be calculated beforehand. Figure 2 shows the four DC-DC converters that will be studied throughout this paper; they are the buck converter, the boost converter, the buck-boost converter, and the KY converter [23], where v_i/i_i and v_o/i_o represent the input and output voltage/current of the converter, respectively, and L represents the inductor, D the diode, S the switch, C the output capacitor, R the loading, C_f the flying capacitor, i_L the inductor current, i_D the diode current, and i_S the switch current. As the equivalent series resistance (ESR) for the passive components are usually small due to high Q design, which are neglected in this paper for simplification. Thus, the left-hand plane zero caused by the ESR of the output capacitor C will not present in the small signal transfer functions for different DC-DC converters.

For calculating the necessary DC parameters of different DC-DC converters, we can just input different V_{on} and V_{off} into (5) and (6). For the buck converter, $V_{on} = V_i - V_o$ and $V_{off} = -V_o$; for the boost converter, $V_{on} = V_i$ and $V_{off} = V_i - V_o$; for the buck-boost converter, $V_{on} = V_i$ and $V_{off} = -V_o$, and for the KY converter, $V_{on} = 2V_i - V_o$ and $V_{off} = V_i - V_o$. On the other hand, using $M = V_o/V_i$ to denote the voltage gain, then D_2 and I_L can be calculated via (5) and (6), as summarized in Table 2.

For the DC relationship between D_1 and M, according to [4], the DC relationships among the inductor current i_L, the switch current i_S, and the diode current i_D are

$$I_S = \frac{D_1}{D_1 + D_2} I_L, \tag{7}$$

$$I_D = \frac{D_2}{D_1 + D_2} I_L. \tag{8}$$

For different DC-DC converters' configurations as in Figure 2, the output current $I_o = I_L$ for the buck and the KY converters and $I_o = I_D$ for the boost and the buck-boost converters. With the D_2 and I_L in Table 2 and the help of (7) and (8), the relationship between D_1 (expressed as $D_1^2 T_s R/2L$) and M can be calculated as presented in Table 2. These parameters are essential for the small-signal transfer function calculation as shown in Sections 4 and 5.

3. Calculation of the Small-Signal Relationship with the Proposed Differentiation Method

If f is a large-signal function of some variables $x, y,$ and $z,$ to attain the small-signal model of these variables, we can express them as the sums of DC and small signal components [10],

$$f = F + \hat{f}, \tag{9}$$

$$x = X + \hat{x}, \tag{10}$$

$$y = Y + \hat{y}, \tag{11}$$

$$z = Z + \hat{z}. \tag{12}$$

By neglecting the DC terms and the high-order small signal terms, we can realize the linear approximation. During the small signal calculation, the following approximation can be used:

$$\frac{1}{1 + \hat{x}} \approx 1 - \hat{x}. \tag{13}$$

For example, the large-signal inductor current of the buck converter given by Kazimierczuk [10] is shown in (14), which can also be given by referring to the expression of I_L in Table 2 and replacing all DC quantities with large-signal quantities. The basis for this replacement is that large-signal analysis is based on DC relationship of circuit variables [10, 15, 19, 21]:

$$i_L = \frac{d_1^2 T_s v_i (1 - m)}{2Lm}, \tag{14}$$

where m denotes the large-signal voltage gain and v_i denotes the small signal input voltage. Expressing the variables as the sums of DC and AC components as (9)–(12) do yield (15), after cancelling the DC components, the small signal expression of the inductor current $\hat{i}_L$ will become (16):
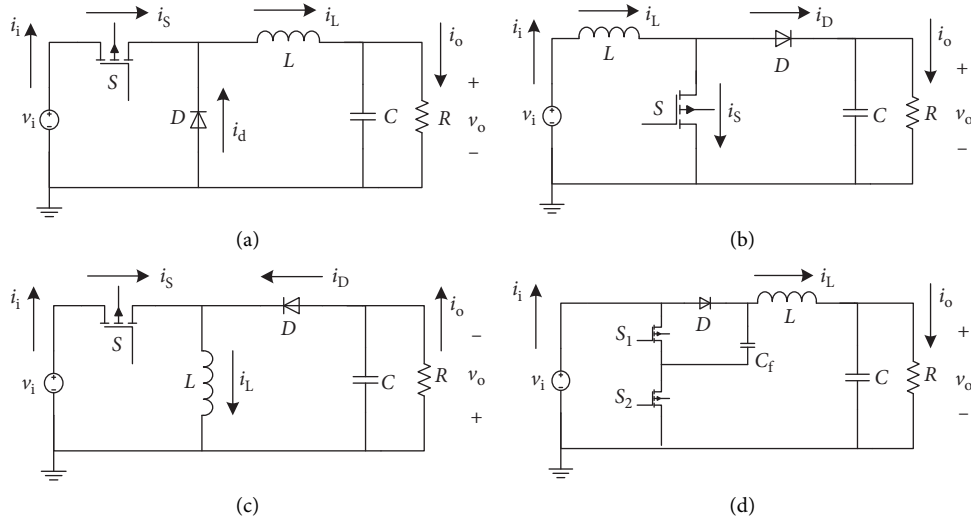
FIGURE 2: Circuit configuration of (a) buck, (b) boost, (c) buck-boost, and (d) KY converters.

TABLE 2: DC parameters for different DC-DC converters.

DC-DC converter	D_2	I_L	$(D_1^2 T_s R)/(2L)$
Buck	$((1-M)/M)D_1$	$(D_1^2 T_s V_i (1-M))/(2LM)$	$(M^2/(1-M))$
Boost	$(1/(M-1))D_1$	$(D_1^2 T_s V_i M)/(2L(M-1))$	$M^2 - M$
Buck-boost	$(1/M)D_1$	$(D_1^2 T_s V_i (1+M))/(2LM)$	M^2
KY	$((2-M)/(M-1))D_1$	$D_1^2 T_s V_i (2-M)/2L(M-1)$	$(M(M-1))/(2-M)$

$$I_L + \hat{i}_L = \frac{(D_1 + \hat{d}_1)^2 T_s (V_i + \hat{v}_i)(1 - M - \hat{m})}{2L(M + \hat{m})}$$

$$\approx \frac{T_s (D_1^2 + 2D_1 \hat{d}_1)(V_i + \hat{v}_i)(1 - M - \hat{m})(1 - (\hat{m}/M))}{2LM}, \tag{15}$$

$$\hat{i}_L = \frac{T_s \left[2D_1 V_i (1-M)\hat{d}_1 + D_1^2 (1-M)\hat{v}_i - D_1^2 V_i \hat{m} - D_1^2 V_i (1-M)(\hat{m}/M) \right]}{2LM}$$

$$= \frac{D_1 T_s V_i (1-M)}{LM} \hat{d}_1 + \frac{D_1^2 T_s (1-M)}{2LM} \hat{v}_i - \frac{D_1^2 T_s V_i}{2LM^2} \hat{m}. \tag{16}$$

However, the above deduction process is quite complicated and time-consuming. To simplify the analysis, we can utilize the calculation of the small signal perturbation as shown in Figure 3.

With a small variation of $\hat{x}$, the corresponding variation of $\hat{f}$ is also very small such that the value $\hat{f}/\hat{x}$ is equal to the derivative of f to x, thus yielding

$$\hat{f} = f_x' \hat{x} + f_y' \hat{y} + f_z' \hat{z}. \tag{17}$$

Following (17) and taking the derivative of (14) with respect to each variable, we can easily get

$$\hat{i}_L = \frac{D_1 T_s V_i (1-M)}{LM} \hat{d}_1 + \frac{D_1^2 T_s (1-M)}{2LM} \hat{v}_i - \frac{D_1^2 T_s V_i}{2LM^2} \hat{m}, \tag{18}$$

where the results in (16) and (18) are equivalent. In the following section, we will use the proposed differentiation method (17) to calculate the small signal relationship.

4. Improved State-Space Averaging Method for Large-Signal and Small Signal Modeling Deduction

In this section, the approach for deducing the DCM small signal models for different DC-DC converters by using the improved SSA method will be discussed.

4.1. General Large-Signal and Corresponding Small Signal Modeling Using the SSA Method. According to the conclusion from [10], the large-signal value relationship and the DC value relationship are identical. Then, (2) and (3) lead to the following large-signal duty ratio d_2:

$$d_2 = \frac{2Li_L}{v_{on} d_1 T_s} - d_1. \tag{19}$$

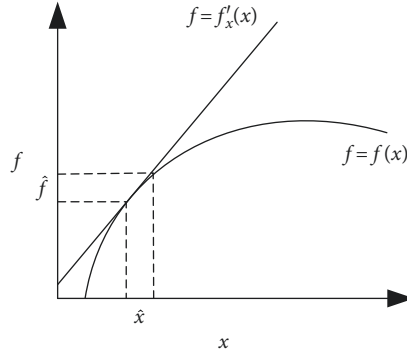By applying the SSA to the inductor voltage and using (19), we get

FIGURE 3: Small signal perturbation.

$$L\frac{di_{\text{L}}}{dt} = v_{\text{on}}d_1 + v_{\text{off}}d_2 = (v_{\text{on}} - v_{\text{off}})d_1 + \frac{2v_{\text{off}}Li_{\text{L}}}{v_{\text{on}}d_1T_{\text{s}}}. \quad (20)$$

Taking the derivative of (20) with respect to v_{on}, v_{off}, d_1, and i_{L}, which are variables in (20), and using (6), we will have the corresponding small signal model given by

$$L\frac{\widehat{di_{\text{L}}}}{dt} = \left(\frac{2V_{\text{on}} - V_{\text{off}}}{V_{\text{on}}}D_1\right)\widehat{v}_{\text{on}} + \left(-\frac{V_{\text{on}}}{V_{\text{off}}}D_1\right)\widehat{v}_{\text{off}}$$

$$+ 2(V_{\text{on}} - V_{\text{off}})\widehat{d}_1 + \left(\frac{V_{\text{off}} - V_{\text{on}}}{I_{\text{L}}}D_1\right)\widehat{i}_{\text{L}}. \quad (21)$$

Then, using the SSA to the capacitor current yields

$$C\frac{du_{\text{C}}}{dt} = i_{\text{o}} - \frac{u_{\text{C}}}{R}. \quad (22)$$

If $i_{\text{o}} = i_{\text{L}}$, and taking the derivative of (22), the corresponding small signal model becomes

$$C\frac{\widehat{du}_{\text{C}}}{dt} = \widehat{i}_{\text{L}} - \frac{\widehat{u}_{\text{C}}}{R}. \quad (23)$$

If $i_{\text{o}} = i_{\text{D}}$, then (8), (19), and (22) lead to

$$C\frac{du_{\text{C}}}{dt} = i_{\text{L}} - \frac{d_1^2 T_{\text{s}} v_{\text{on}}}{2L} - \frac{u_{\text{C}}}{R}. \quad (24)$$

Finally, taking the derivative of (24), we obtain the corresponding small signal model as follows:

$$C\frac{\widehat{du}_{\text{C}}}{dt} = \widehat{i}_{\text{L}} - \frac{D_1 T_{\text{s}} V_{\text{on}}}{L}\widehat{d}_1 - \frac{D_1^2 T_{\text{s}}}{2L}\widehat{v}_{\text{on}} - \frac{\widehat{u}_{\text{C}}}{R}, \quad (25)$$

where (21), (23), and (25) are the three general equations for deducing the DCM small signal models of different DC-DC converters. Then, after input, the values of the inductor

voltage drops during the charging (V_{on}) and discharging (V_{off}) cycles, as well as the DC parameters of each DC-DC converter from Table 2, into (21), (23), and (25), and the corresponding DCM small signal models can be deduced easily, as detailed next.

4.2. Buck Converter Small Signal Transfer Function. For the buck converter, $V_{\text{on}} = V_{\text{o}} - V_{\text{o}}$, $V_{\text{off}} = -V_{\text{o}}$, and $i_{\text{o}} = i_{\text{L}}$. Besides, Table 2 gives $I_{\text{L}} = (D_1^2 T_{\text{s}} V_{\text{i}}(1 - M))/(2LM)$ and $(D_1^2 T_{\text{s}} R)/(2L) = (M^2)/(1 - M)$, and substituting them into (21) and (23), gives

$$L\frac{\widehat{di_{\text{L}}}}{dt} = \left(\frac{2V_{\text{i}} - V_{\text{o}}}{V_{\text{i}} - V_{\text{o}}}D_1\right)(\widehat{v}_{\text{i}} - \widehat{v}_{\text{o}})$$

$$-\left(\frac{V_{\text{i}} - V_{\text{o}}}{V_{\text{o}}}D_1\right)\widehat{v}_{\text{o}} + 2V_{\text{i}}\widehat{d}_1 - \frac{V_{\text{i}}}{I_{\text{L}}}D_1\widehat{i}_{\text{L}}, \quad (26)$$

$$C\frac{\widehat{du}_{\text{C}}}{dt} = \widehat{i}_{\text{L}} - \frac{\widehat{u}_{\text{C}}}{R}. \quad (27)$$

Let $\widehat{v}_{\text{i}} = 0$, then (26) becomes

$$\left(sL + \frac{2LM}{D_1 T_{\text{s}}(1 - M)}\right)\widehat{i}_{\text{L}} = \frac{1}{M^2 - M}D_1\widehat{v}_{\text{o}} + 2V_{\text{i}}\widehat{d}_1. \quad (28)$$

Further, if $u_{\text{c}} = v_{\text{o}}$, then (27) will be

$$\left(sC + \frac{1}{R}\right)\widehat{v}_{\text{o}} = \widehat{i}_{\text{L}}. \quad (29)$$

Considering (28) and (29) simultaneously, the transfer function (V_{o} over d_1) of the buck converter can be obtained as

$$\frac{\widehat{v}_{\text{o}}(s)}{\widehat{d}_1(s)} = \frac{2V_{\text{i}}}{s^2 LC + s\left((L/R) + (2LCM)/(D_1 T_{\text{s}}(1 - M))\right) + \left((2 - M)D_1\right)/((1 - M)M)}. \quad (30)$$

4.3. Boost Converter Small Signal Transfer Function. For the boost converter, $V_{on} = V_i$, $V_{off} = V_i - V_o$, and $i_o = i_D$, and Table 2 gives $I_L = (D_1^2 T_s V_i M)/(2L(M-1))$ and $(D_1^2 T_s R)/(2L) = M^2 - M$; by substituting them into (21) and (25), it leads to

$$L\frac{d\hat{i}_L}{dt} = \left(\frac{V_i + V_o}{V_i}D_1\right)\hat{v}_i - \left(\frac{V_i}{V_i - V_o}D_1\right)(\hat{v}_i - \hat{v}_o)$$

$$+ 2V_o\hat{d}_1 - \frac{V_o}{I_L}D_1\hat{i}_L, \tag{31}$$

$$C\frac{d\hat{u}_C}{dt} = \hat{i}_L - \frac{D_1 T_s V_i}{L}\hat{d}_1 - \frac{D_1^2 T_s}{2L}\hat{v}_i - \frac{\hat{u}_C}{R}. \tag{32}$$

Let $\hat{v}_i = 0$, then (31) will be

$$\left(sL + \frac{2L(M-1)}{D_1 T_s}\right)\hat{i}_L = \frac{1}{1-M}D_1\hat{v}_o + 2V_o\hat{d}_1, \tag{33}$$

and if $u_c = v_o$ and $\hat{v}_i = 0$, then we can obtain the following equation from (32):

$$\left(sC + \frac{1}{R}\right)\hat{v}_o + \frac{D_1 T_s V_i}{L}\hat{d}_1 = \hat{i}_L. \tag{34}$$

Also considering (33) and (34) simultaneously, in this case, the transfer function of the boost converter will become

$$\frac{\hat{v}_o(s)}{\hat{d}_1(s)} = \frac{D_1 T_s V_i ((2)/(D_1 T_s)) - s)}{s^2 LC + s((L/R) + ((2LC(M-1))/(D_1 T_s))) + ((2M-1)D_1)/(M(M-1))}. \tag{35}$$

4.4. Buck-Boost Converter Small Signal Transfer Function. For the boost converter, $V_{on} = V_i$, $V_{off} = -V_o$, and $i_o = i_D$, and from Table 2, $I_L = (D_1^2 T_s V_i(1+M))/(2LM)$ and $(D_1^2 T_s R)/(2L) = M^2$. Then, by substituting them into (21) and (25), we have

$$L\frac{d\hat{i}_L}{dt} = \left(\frac{2V_i + V_o}{V_i}D_1\right)\hat{v}_i - \frac{V_i}{V_o}D_1\hat{v}_o$$

$$+ 2(V_i + V_o)\hat{d}_1 - \frac{(V_i + V_o)}{I_L}D_1\hat{i}_L, \tag{36}$$

$$C\frac{d\hat{u}_C}{dt} = \hat{i}_L - \frac{D_1 T_s V_i}{L}\hat{d}_1 - \frac{D_1^2 T_s}{2L}\hat{v}_i - \frac{\hat{u}_C}{R}. \tag{37}$$

With $\hat{v}_i = 0$, then (36) will lead to

$$\left(sL + \frac{2LM}{D_1 T_s}\right)\hat{i}_L = -\frac{1}{M}D_1\hat{v}_o + 2(V_i + V_o)\hat{d}_1, \tag{38}$$

and again if $u_c = v_o$ and $\hat{v}_i = 0$, (37) yields

$$\left(sC + \frac{1}{R}\right)\hat{v}_o + \frac{D_1 T_s V_i}{L}\hat{d}_1 = \hat{i}_L. \tag{39}$$

Finally, considering (38) and (39) simultaneously, again the transfer function of the buck-boost converter will be

$$\frac{\hat{v}_o(s)}{\hat{d}_1(s)} = \frac{D_1 T_s V_i ((2/(D_1 T_s)) - s)}{s^2 LC + s((L/R) + ((2LCM)/(D_1 T_s))) + ((2D_1)/M)}. \tag{40}$$

4.5. KY Converter Small Signal Transfer Function. For the KY converter, $V_{on} = 2V_i - V_o$, $V_{off} = V_i - V_o$, and $i_o = i_L$, and from Table 2, $I_L = (D_1^2 T_s V_i(2-M))/(2L(M-1))$ and $(D_1^2 T_s R)/(2L) = (M(M-1))/(2-M)$. Then, substituting them into (21) and (23) will lead to

$$L\frac{d\hat{i}_L}{dt} = \frac{3V_i - V_o}{2V_i - V_o}D_1(2\hat{v}_i - \hat{v}_o)$$

$$-\frac{2V_i - V_o}{V_i - V_o}D_1(\hat{v}_i - \hat{v}_o) + 2V_i\hat{d}_1 - \frac{V_i}{I_L}D_1\hat{i}_L, \tag{41}$$

$$C\frac{d\hat{u}_C}{dt} = \hat{i}_L - \frac{\hat{u}_C}{R}. \tag{42}$$

Let $\hat{v}_i = 0$, then (41) becomes

$$\left(sL + \frac{2L(M-1)}{D_1 T_s(2-M)}\right)\hat{i}_L = \frac{1}{((2-M)(1-M))}D_1\hat{v}_o + 2V_i\hat{d}_1. \tag{43}$$

Then with $u_c = v_o$, (42) gives

$$\left(sC + \frac{1}{R}\right)\hat{v}_o = \hat{i}_L. \tag{44}$$

Again with (43) and (44) considered simultaneously, the transfer function of the KY converter can be obtained as

$$\frac{\hat{v}_o(s)}{\hat{d}_1(s)} = \frac{2V_i}{s^2 LC + s((L/R) + (2LC(M-1))/(D_1 T_s(2-M)))) + ((M^2 - 4M + 2)D_1)/((2-M)(1-M)M)}. \tag{45}$$

5. Circuit Averaging Method for Large-Signal and Small Signal Modeling Deduction

In this section, the approach for deducing the DCM small signal models for different DC-DC converters by using the CA method will be discussed.

5.1. General Large-Signal and Corresponding Small Signal Modeling Using the CA Method. With the help of Reference [10], according to (7) and (8), the switching network of the DC-DC converter can be transformed into the circuit as shown in Figure 4.

When the circuit reaches the steady-state, the average voltage across the inductor is zero, then Figure 4 imposes,

$$V_{LM} = 0. \tag{46}$$

From Figure 4, we can obtain

$$V_{LS} = V_{LM} + V_{MS} = V_{MS}, \tag{47}$$

$$V_{LD} = V_{LM} + V_{MD} = V_{MD}. \tag{48}$$

By using (5)–(8), they yield the following large-signal equations (considering identical the large-signal value and the DC value relationships):

$$i_S = \frac{d_1^2 T_s v_{on}}{2L}, \tag{49}$$

$$i_D = -\frac{d_1^2 T_s v_{on}^2}{2L v_{off}}. \tag{50}$$

Taking the derivative of (49) and (50), the corresponding small signal equations will emerge as follows:

$$\begin{aligned} \widehat{i}_S &= \frac{D_1 T_s V_{on}}{L}\widehat{d}_1 + \frac{D_1^2 T_s}{2L}\widehat{v}_{on}, \\ \widehat{i}_D &= -\frac{D_1 T_s V_{on}^2}{L V_{off}}\widehat{d}_1 - \frac{D_1^2 T_s V_{on}}{L V_{off}}\widehat{v}_{on} + \frac{D_1^2 T_s V_{on}^2}{2L V_{off}^2}\widehat{v}_{off}, \end{aligned} \tag{51}$$

and from (47) and (48), $V_{on} = V_{LS} = V_{MS}$ and $V_{off} = V_{LD} = V_{MD}$. Then, the small signal circuit of the switching network in Figure 4 can be transformed into Figure 5, where

$$\begin{aligned} k_S &= \frac{D_1 T_s V_{on}}{L}, \\ g_S &= \frac{D_1^2 T_s}{2L}, \\ k_D &= -\frac{D_1 T_s V_{on}^2}{L V_{off}}, \\ g_D &= -\frac{D_1^2 T_s V_{on}}{L V_{off}}, \\ g_M &= \frac{D_1^2 T_s V_{on}^2}{2L V_{off}^2}. \end{aligned} \tag{52}$$

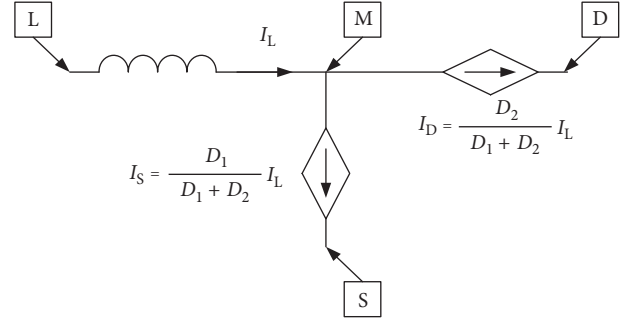From Figure 5, we can write

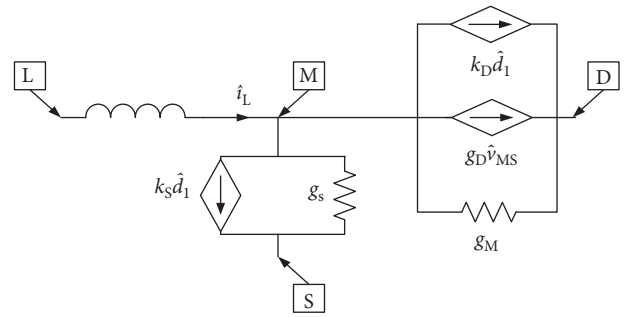FIGURE 4: Equivalent circuit of the switching network (current source).

FIGURE 5: Small signal equivalent circuit of the switching network.

$$\begin{aligned} \widehat{i}_L &= (k_S + k_D)\widehat{d}_1 + (g_S + g_D)\widehat{v}_{MS} + g_M\widehat{v}_{MD}, \\ &= (k_S + k_D)\widehat{d}_1 + (g_S + g_D + g_M)\widehat{v}_{MS} + g_M\widehat{v}_{SD}. \end{aligned} \tag{53}$$

Then, with $k_{d1} = k_S + k_D$ and $g_{MS} = g_S + g_D + g_M$, we can obtain the factors $k_S, k_D, k_{d1}, g_S, g_D, g_M,$ and g_{MS} of the four DC-DC converters (buck, boost, buck-boost, and KY) as shown in Table 3.

With these factors, we can substantially simplify the calculation process, as shown next. Further, we can deduce that

$$\widehat{v}_{LM} = sL\widehat{i}_L, \tag{54}$$

$$\widehat{v}_{MS} = \widehat{v}_{LS} - \widehat{v}_{LM}. \tag{55}$$

Then (53) can be rewritten as

$$\left(sL + \frac{1}{g_{MS}}\right)\widehat{i}_L = \frac{k_{d_1}}{g_{MS}}\widehat{d}_1 + \widehat{v}_{LS} + \frac{g_M}{g_{MS}}\widehat{v}_{SD}, \tag{56}$$

and considering the capacitor, its current becomes

$$C\frac{d\widehat{u}_C}{dt} = \widehat{i}_o - \frac{\widehat{u}_C}{R}. \tag{57}$$

If $i_o = i_L$, (57) will become

$$C\frac{d\widehat{u}_C}{dt} = \widehat{i}_L - \frac{\widehat{u}_C}{R}. \tag{58}$$

Then, with $u_c = v_o$, we have

TABLE 3: Relevant factors of the circuit averaging (CA) method.

DC-DC converter	Buck	Boost	Buck-boost	KY
k_S	$(2M^2 V_i)/(D_1 R)$	$(2M(M-1)V_i)/(D_1 R)$	$(2M^2 V_i)/(D_1 R)$	$(2M(M-1)V_i)/(D_1 R)$
k_D	$((2M(1-M)V_i)/(D_1 R))$	$(2MV_i)/(D_1 R)$	$(2MV_i)/(D_1 R)$	$(2M(2-M)V_i)/(D_1 R)$
k_{d1}	$(2MV_i)/(D_1 R)$	$(2M^2 V_i)/(D_1 R)$	$(2M(M+1)V_i)/(D_1 R)$	$(2MV_i)/(D_1 R)$
g_S	$(M^2)/((1-M)R)$	$(M^2-M)/(R)$	M^2/R	$(M(M-1))/((2-M)R)$
g_D	$(2M)/R$	$(2M)/R$	$(2M)/R$	$(2M)/R$
g_M	$(1-M)/R$	$M/((M-1)R)$	$1/R$	$(M(2-M))/((M-1)R)$
g_{MS}	$1/((1-M)R)$	$M^3/((M-1)R)$	$((M+1)^2)/R$	$M/((2-M)(M-1))$

$$\widehat{i}_L = \left(SC + \frac{1}{R}\right)\widehat{v}_o, \tag{59}$$

and with $i_o = i_D$, (57) yields

$$C\frac{d\widehat{u}_C}{dt} = k_D\widehat{d}_1 + g_D\widehat{v}_{MS} + g_M\widehat{v}_{MD} - \frac{\widehat{u}_C}{R}. \tag{60}$$

Finally, with (54)–(56), $u_c = v_o$, (60) can be rewritten as

$$\widehat{i}_L = \frac{g_{MS}}{g_D + g_M}\left(SC + \frac{1}{R}\right)\widehat{v}_o$$
$$+\left(k_{d1} - \frac{k_D \cdot g_{MS}}{g_D + g_M}\right)\widehat{d}_1 + \left(g_M - \frac{g_M \cdot g_{MS}}{g_D + g_M}\right)\widehat{v}_{SD}. \tag{61}$$

Here, (56), (59), and (61) are the 3 general equations to deduce the DCM small signal models for the different DC-DC converters. By just input, the voltage drops V_{LS} and V_{SD} from Figure 5, plus the factors (Table 3) and the DC parameters (Table 2) into (56), (59) and (61), and the corresponding DCM small signal transfer functions can be calculated easily in the following.

5.2. Buck Converter Small Signal Transfer Function. For the buck converter, from Figure 5, $V_{LS} = V_i - V_o$, $V_{SD} = -V_i$, and $i_o = i_L$, and from Table 2, $I_L = (D_1^2 T_s V_i(1-M))/(2LM)$ and $(D^2 T_s R)/(2L) = M^2/(1-M)$. Then, with $\widehat{v}_i = 0$, (56) and (59) lead to

$$(sL + (1-M)R)\widehat{i}_L = \frac{2M(1-M)V_i}{D_1}\widehat{d}_1 - \widehat{v}_o, \tag{62}$$

$$\widehat{i}_L = \left(sC + \frac{1}{R}\right)\widehat{v}_o. \tag{63}$$

And from (62) and (63) simultaneously, the transfer function of the buck converter can be obtained as

$$\frac{\widehat{v}_o(s)}{\widehat{d}_1(s)} = \frac{M(1-M)((2V_i)/D_1)}{s^2 LC + s((L/R) + RC(1-M)) + 2 - M}. \tag{64}$$

5.3. Boost Converter Small Signal Transfer Function. For the boost converter, from Figure 5, $V_{LS} = V_i$, $V_{SD} = -V_o$, $i_o = i_D$, and from Table 2, $I_L = (D_1^2 T_s V_i M)/(2L(M-1))$ and $(D_1^2 T_s R)/(2L) = M^2 - M$. Then, with $\widehat{v}_i = 0$, (56) and (61) imply,

$$\left(sL + \frac{(M-1)R}{M^3}\right)\widehat{i}_L = \frac{2(M-1)V_i}{D_1 M}\widehat{d}_1 - \frac{1}{M^2}\widehat{v}_o, \tag{65}$$

$$\widehat{i}_L = \frac{M^2}{2M-1}\left(sC + \frac{2M-1}{MR}\right)\widehat{v}_o$$
$$+ \frac{2(M-1)M^2 V_i}{(2M-1)D_1 R}\widehat{d}_1. \tag{66}$$

Again, from (65) and (66) simultaneously, the transfer function of the boost converter will become,

$$\frac{\widehat{v}_o(s)}{\widehat{d}_1(s)} = \frac{((D_1 T_s V_i)/M)((2(M-1))/(D_1^2 T_s M)) - s)}{s^2 LC + s(((L(2M-1))/(RM)) + ((RC(M-1))/(M^3))) + ((2M-1)/M^3)}. \tag{67}$$

5.4. Buck-Boost Converter Small Signal Transfer Function. For the buck-boost converter, from Figure 5, $V_{LS} = V_i$, $V_{SD} = -(V_i + V_o)$, and $i_o = i_D$, and from Table 2, $I_L = (D_1^2 T_s V_i(1+M))/(2LM)$ and $(D_1^2 T_s R)/(2L) = M^2$. Then, with $\widehat{v}_i = 0$, (56) and (61) impose

$$\left(sL + \frac{R}{(M+1)^2}\right)\widehat{i}_L = \frac{2MV_i}{D_1(M+1)}\widehat{d}_1 - \frac{1}{(M+1)^2}\widehat{v}_o, \tag{68}$$

$$\widehat{i}_L = \frac{(M+1)^2}{2M+1}\left(SC + \frac{2M^2 + 2M + 1}{(M+1)^2 R}\right)\widehat{v}_o$$
$$+ \frac{2(M^3 + M^2)V_i}{(2M+1)D_1 R}\widehat{d}_1. \tag{69}$$

Similarly, with (68) and (69) considered simultaneously, the transfer function of the buck-boost converter will be

$$\frac{\widehat{v}_o(s)}{\widehat{d}_1(s)} = \frac{\left((D_1 T_s V_i)/(M+1)\right)\left(\left(2M/\left(D_1^2 T_s (M+1)\right)\right)-s\right)}{s^2 LC + s\left(\left(\left(L(2M^2+2M+1)\right)/\left(R(M+1)^2\right)\right)+\left(\left(RC\right)/\left((M+1)^2\right)\right)\right)+\left(2/\left((M+1)^2\right)\right)}. \tag{70}$$

6.5. KY Converter Small Signal Transfer Function.

For the KY converter, from Figure 5, $V_{LS} = 2V_i - V_o$, $V_{SD} = -V_i$, and $i_o = i_L$, and from Table 2, $I_L = (D_1^2 T_s V_i (2-M))/(2L(M-1))$ and $(D_1^2 T_s R)/(2L) = (M(M-1))/((2-M))$. Then, with $\widehat{v}_i = 0$, (56) and (59) entail

$$\left(sL + \frac{(2-M)(M-1)R}{M}\right)\widehat{i}_L = \frac{2(2-M)(M-1)V_i}{D_1}\widehat{d}_1 - \widehat{v}_o, \tag{71}$$

$$\widehat{i}_L = \left(sC + \frac{1}{R}\right)\widehat{v}_o. \tag{72}$$

Finally, from (71) and (72) simultaneously, the transfer function of the KY converter will become

$$\frac{\widehat{v}_o(s)}{\widehat{d}_1(s)} = \frac{(2-M)(M-1)\left((2V_i)/D_1\right)}{s^2 LC + s\left((L/R) + ((RC(2-M)(M-1))/M)\right)+((2-M)(M-1)+M)/M)}. \tag{73}$$

6. Simulation Results

We simulated the four DC-DC converters within a Cadence environment of a 65 nm CMOS process and also MATLAB to verify and compare the accuracy of the small signal transfer functions (30), (35), (40), (45), (64), (67), (70), and (73) deduced by the improved SSA and CA methods.

6.1. Buck Converter.

The relevant parameters of the buck converter (Figure 2) are $V_i = 1.2$ V, $f_s = 100$ MHz, $C = 10$ nF, $L = 36$ nH, and $R = 40\,\Omega$. The Bode plot comparison between the transfer functions with the SSA and the CA methods ((30) and (64)), and the simulated circuit power stage (PS), is shown in Figure 6, for $d_1 = 0.3$, 0.5, and 0.7.

From Figure 6, we can conclude that in the buck converter, the CA method provides higher accuracy than the SSA method in any duty ratio range d_1, with clearer emphasis at larger d_1 values.

6.2. Boost Converter.

The relevant parameters of the boost converter (Figure 2) are $V_i = 1.2$ V, $f_s = 100$ MHz, $C = 10$ nF, $L = 13.5$ nH, and $R = 60\,\Omega$. The Bode plot comparison between the transfer functions with the SSA and the CA methods ((35) and (67)), and the simulated circuit PS, is shown in Figure 7, for $d_1 = 0.3$, 0.5, and 0.7.

From Figure 7, we can conclude that in the boost converter with a small duty ratio value ($d_1 = 0.3$), the SSA method contains slightly better accuracy than the CA method. But, as the d_1 increases, the accuracy of the CA method will improve over the SSA method, again being more evident for larger d_1 values.

6.3. Buck-Boost Converter.

The relevant parameters of the buck-boost converter (Figure 2) are $V_i = 1.2$ V, $f_s = 100$ MHz, $C = 40$ nF, $L = 15$ nH, and $R = 150\,\Omega$. The Bode plot comparison between the transfer functions with the SSA and

the CA methods ((40) and (70)), and the simulated circuit PS, is shown in Figure 8, for $d_1 = 0.3$, 0.5, and 0.7.

From Figure 8, the analysis of the simulation results of the boost converter is similar to those of the buck-boost converter, leading exactly to the same conclusions.

6.4. KY Converter.

Finally, for the KY converter (Figure 2), $V_i = 1.2$ V, $f_s = 100$ MHz, $C = 10$ nF, $C_f = 10$ nF, $L = 3.6$ nH, and $R = 60\,\Omega$, and the Bode plot comparison between the transfer functions with the SSA and the CA methods ((45) and (73)), and the simulated circuit PS, is shown in Figure 9, for $d_1 = 0.3$, 0.5, and 0.7.

From Figure 9, the analysis of the simulation results of the KY converter are similar to those of the buck converter, leading exactly to the same conclusions.

7. High-Accuracy Modeling Method for Different DC-DC Converters in DCM—Selection Strategy

7.1. Derivation.

By using the methods presented in [3] and [6], the approximate poles and zeros for different DC-DC converters in DCM with the SSA and CA methods can be calculated and summarized in Table 4. The previous Bode plot simulation results clearly demonstrate that the phase-frequency responses of the DC-DC converters power stages generally show a larger phase lag than the small signal models given by both the SSA and CA methods. Based on this, if the modeling method presents a smaller value of the second pole or zero (leading to a larger phase lag), it will exhibit a better accuracy of the system phase-frequency response. From Table 4, we propose a selection strategy of high-accuracy small signal modeling method for the DC-DC converters as in Table 5.

7.2. Verification.

For verification of the proposed selection strategy, we simulated a buck converter and a boost
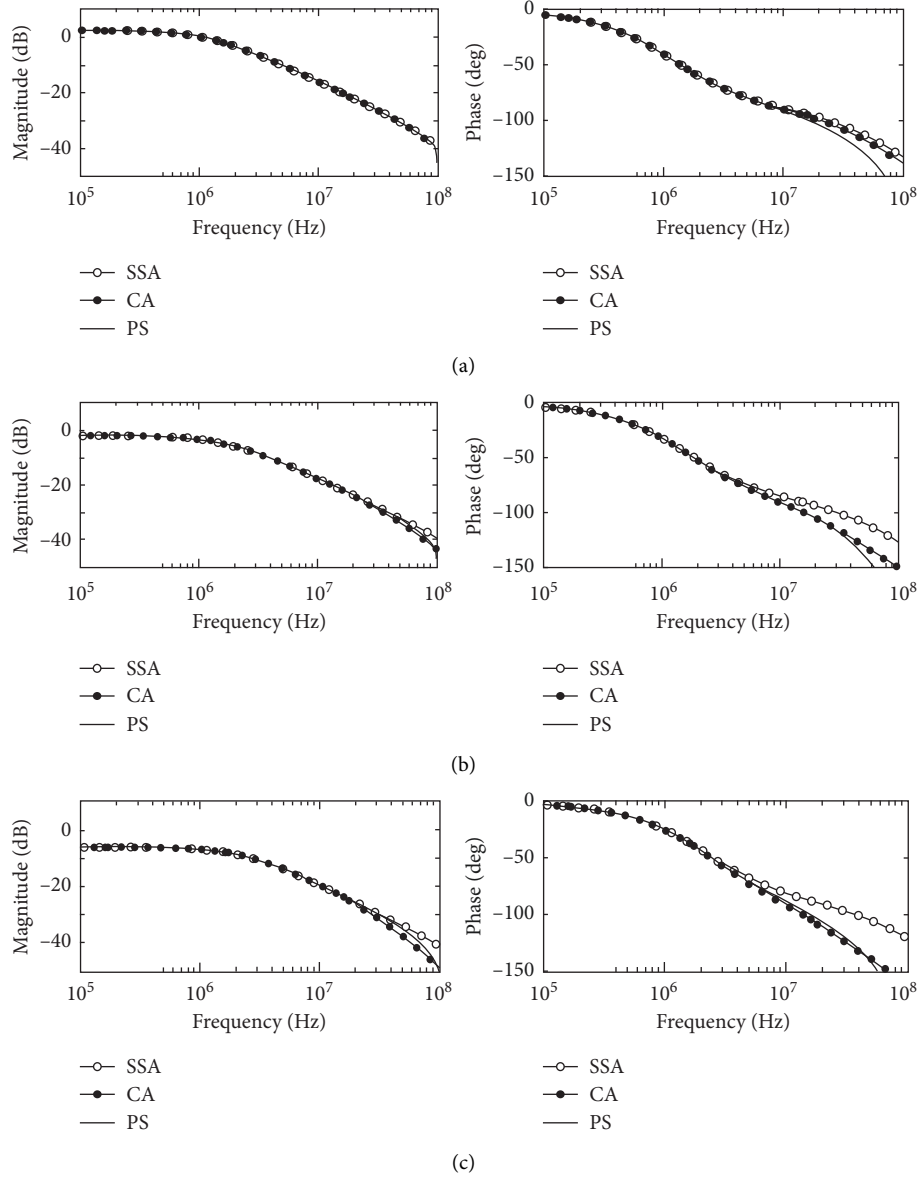
(a)

(b)

(c)

FIGURE 6: Small signal models comparison of the buck converter with SSA and CA methods: (a) $d_1 = 0.3$; (b) $d_1 = 0.5$; and (c) $d_1 = 0.7$.
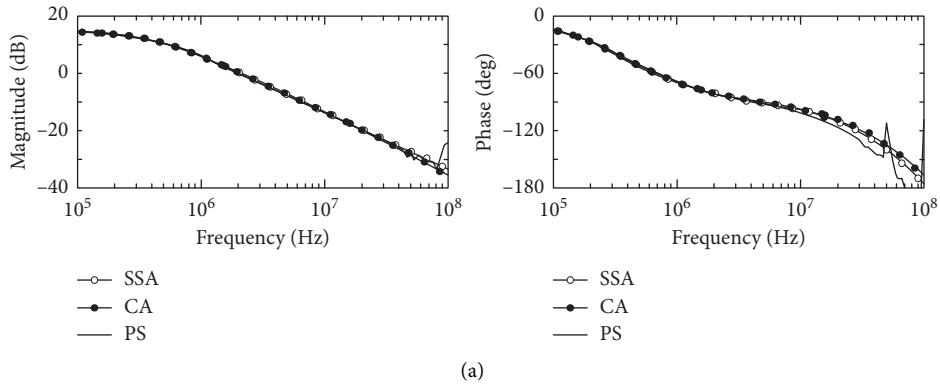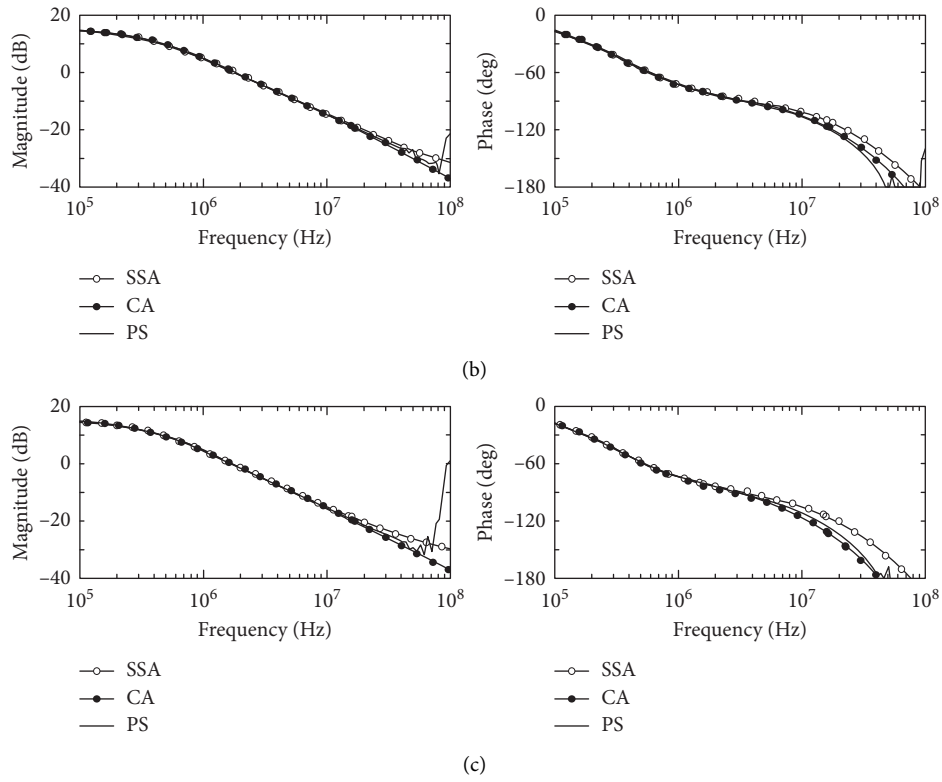

(a)

FIGURE 7: Continued.

(b)

(c)

Figure 7: Small signal models comparison of the boost converter with SSA and CA methods: (a) $d_1 = 0.3$; (b) $d_1 = 0.5$; and (c) $d_1 = 0.7$.
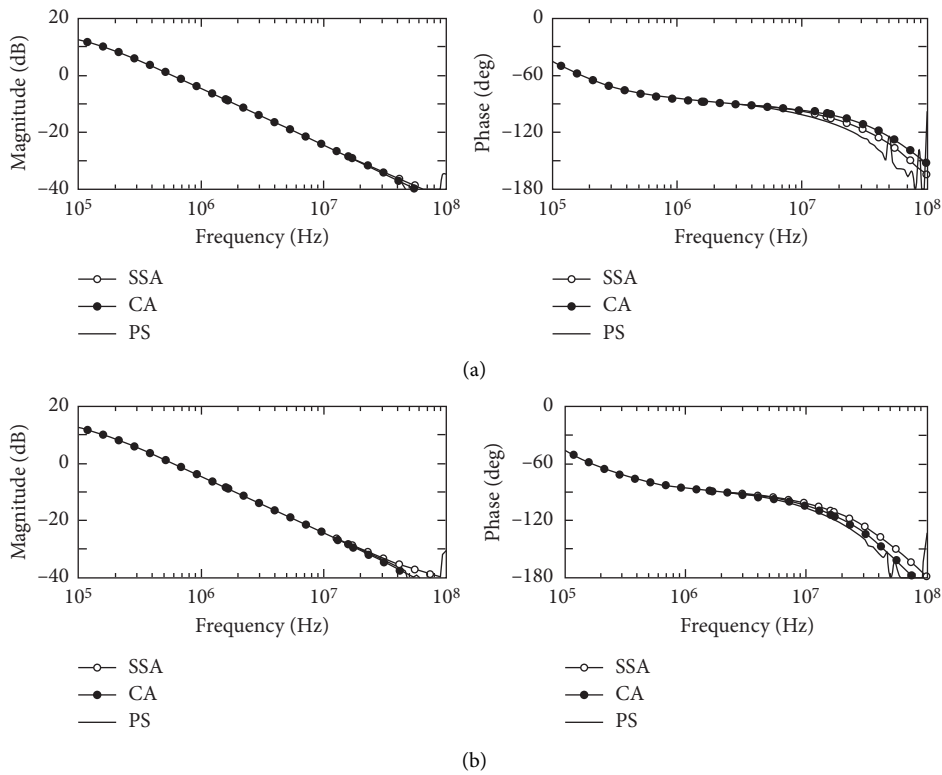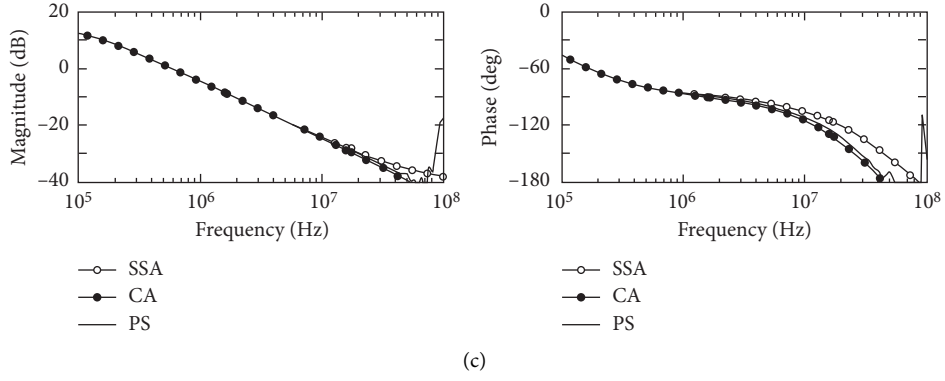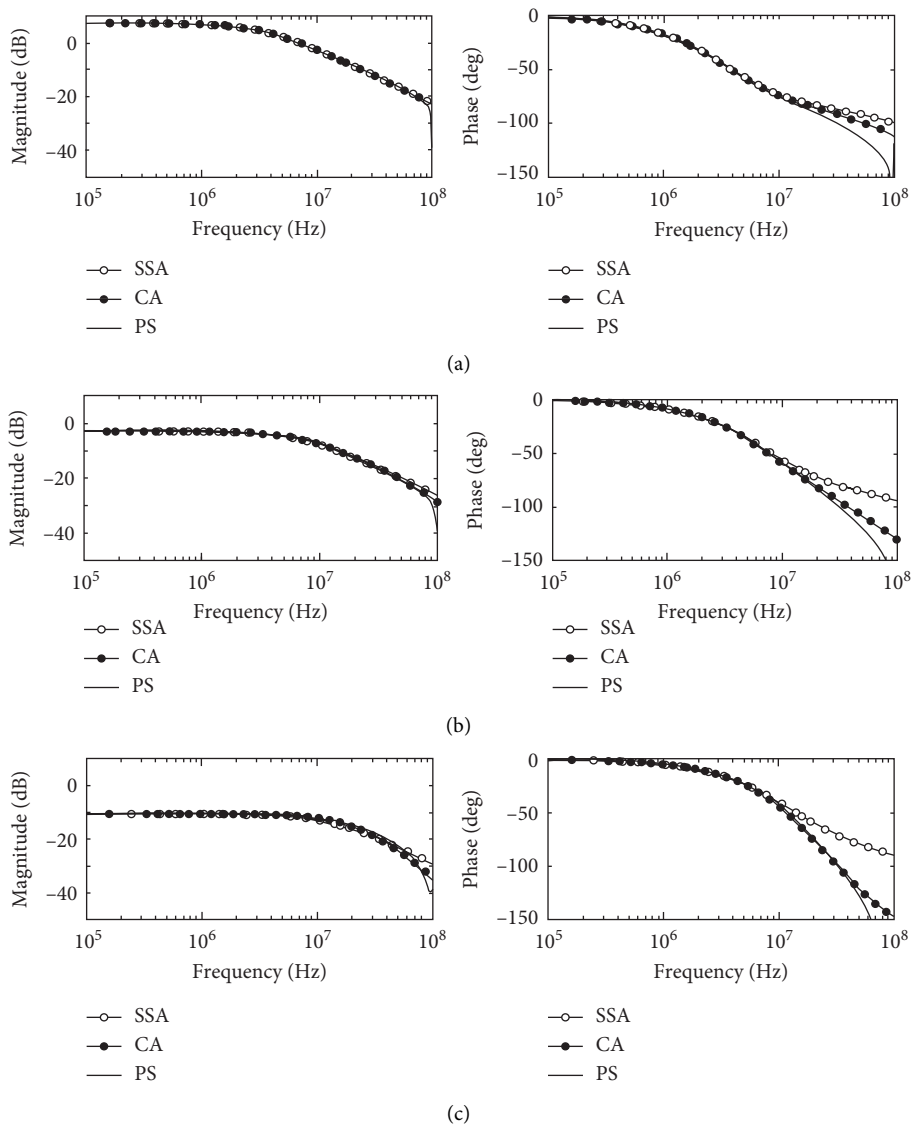

(a)

(b)

Figure 8: Continued.

(c)

FIGURE 8: Small signal models comparison of the buck-boost converter with SSA and CA methods: (a) $d_1 = 0.3$; (b) $d_1 = 0.5$; and (c) $d_1 = 0.7$.

(a)

(b)

(c)

FIGURE 9: Small signal models comparison of the KY converter with SSA and CA methods: (a) $d_1 = 0.3$; (b) $d_1 = 0.5$; and (c) $d_1 = 0.7$.

converter with the Cadence Spectre simulator to demonstrate that the converter operates with higher stability with a more accurate small signal modeling method used in the

compensator design. The simulated results of the system phase-frequency response and the closed-loop controlled converters' load transient response are presented in

TABLE 4: Approximate poles and zeros for various DC-DC converters in DCM.

Name	Method	First pole	Second pole	Zero
Buck	SSA	$(2 - M)/(RC(1 - M))$	$(2M)/(d_1 T_s (1 - M))$	
	CA	$(2 - M)/(RC(1 - M))$	$(2M^2)/(d_1^2 T_s)$	
Boost	SSA	$(2M - 1)/(RC(M - 1))$	$(2(M - 1))/(d_1 T_s)$	$2/(d_1 T_s)$
	CA	$(2M - 1)/(RC(M - 1))$	$(2((M - 1)/M)^2)/(d_1^2 T_s)$	$(2((M - 1)/M))/(d_1^2 T_s)$
Buck-boost	SSA	$2/(RC)$	$(2M)/(d_1 T_s)$	$2/(d_1 T_s)$
	CA	$2/(RC)$	$2(M/(M + 1))^2/d_1^2 T_s$	$2(M/(M + 1))/d_1^2 T_s$
KY	SSA	$(M^2 - 4M + 2)/(RC(M^2 - 3M + 2))$	$(2(M - 1))/(d_1 T_s (2 - M))$	
	CA	$(M^2 - 4M + 2)/(RC(M^2 - 3M + 2))$	$(2(M - 1)^2)/(d_1^2 T_s)$	

TABLE 5: Selection strategy between SSA and CA for high-accuracy small signal modeling.

Name	Criterion	Modeling selection
Buck	$(2M/(d_1 T_s (1 - M))) < ((2M^2)/(d_1^2 T_s))$	SSA
	$(2M/(d_1 T_s (1 - M))) > ((2M^2)/(d_1^2 T_s))$	CA
Boost	$\min(((2(M - 1))/(d_1 T_s)), (2/d_1 T_s)) < (2((M - 1)/M)^2/(d_1^2 T_s))$	SSA
	$\min(((2(M - 1))/(d_1 T_s)), (2/d_1 T_s)) > (2((M - 1)/M)^2/(d_1^2 T_s))$	CA
Buck-boost	$\min(((2M)/(d_1 T_s)), (2/d_1 T_s)) < (2(M/(M + 1))^2/(d_1^2 T_s))$	SSA
	$\min(((2M)/(d_1 T_s)), (2/d_1 T_s)) > (2(M/(M + 1))^2/(d_1^2 T_s))$	CA
KY	$(2(M - 1))/(d_1 T_s (2 - M)) < ((2(M - 1)^2)/(d_1^2 T_s))$	SSA
	$(2(M - 1))/(d_1 T_s (2 - M)) > ((2(M - 1)^2)/(d_1^2 T_s))$	CA
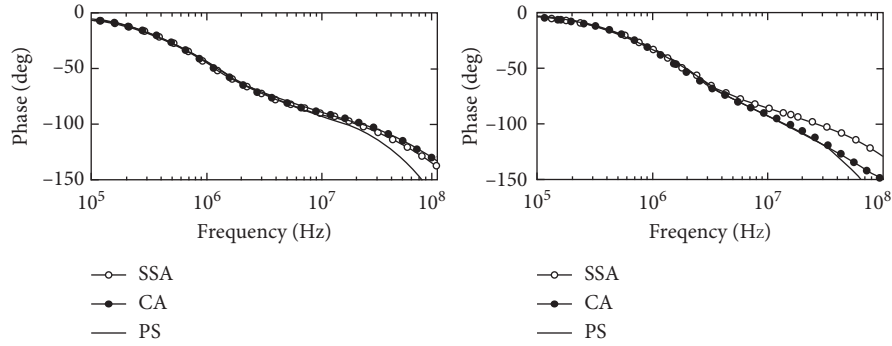
FIGURE 10: Simulation verification with the buck converter ($V_i = 1.2$ V, $f_s = 100$ MHz, $C = 10$ nF, $L = 40$ nH, and $R = 40\,\Omega$): (a) $d_1 = 0.2$, $(2M/(d_1 T_s (1 - M))) < ((2M^2)/(d_1^2 T_s))$; and (b) $d_1 = 0.5$, $(2M/(d_1 T_s (1 - M))) > ((2M^2)/(d_1^2 T_s))$.
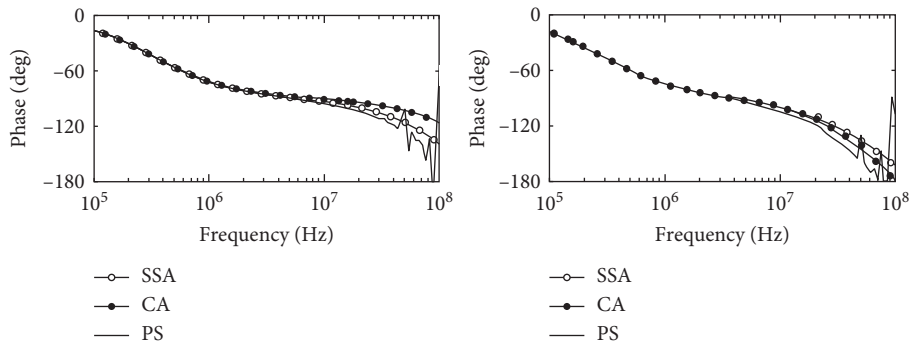
FIGURE 11: Simulation verification with the boost converter ($V_i = 1.2$ V, $f_s = 100$ MHz, $C = 20$ nF, $L = 2$ nH, and $R = 15\,\Omega$): (a) $d_1 = 0.2$, $\min(((2(M - 1))/(d_1 T_s)), (2/d_1 T_s)) < (2((M - 1)/M)^2/(d_1^2 T_s))$; and (b) $d_1 = 0.5$, $\min(((2(M - 1))/(d_1 T_s)), (2/d_1 T_s)) > (2((M - 1)/M)^2/(d_1^2 T_s))$.
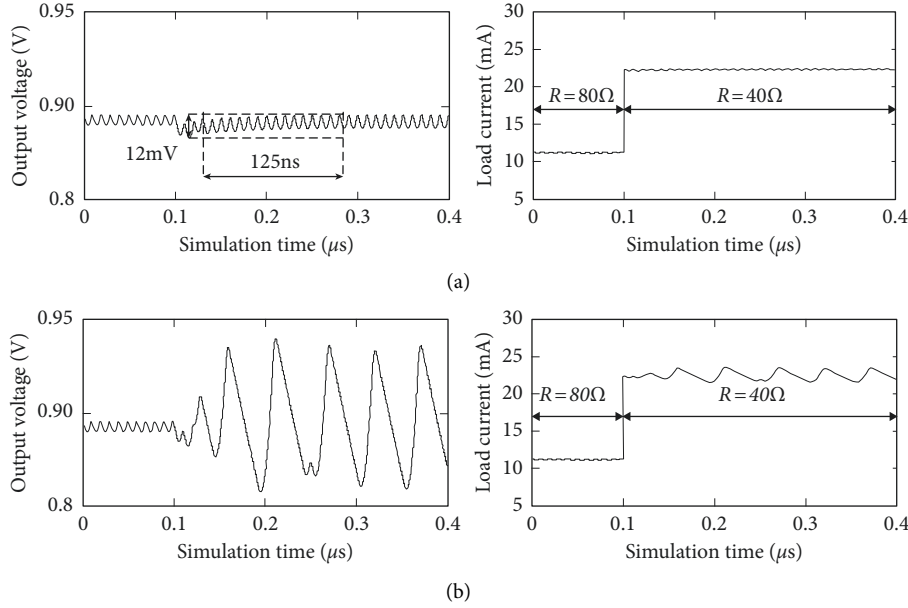
(a)

(b)

FIGURE 12: V_o and i_o of the designed buck converter with $((2M)/(d_1 T_s(1-M))) > (2M^2/d_1^2 T_s)$ ($V_i = 1.2$ V, $f_s = 100$ MHz, $C = 10$ nF, $L = 40$ nH, and $R = 80/40\,\Omega$) and PM = 45°. (a) Compensator based on CA. (b) Compensator based on SSA.
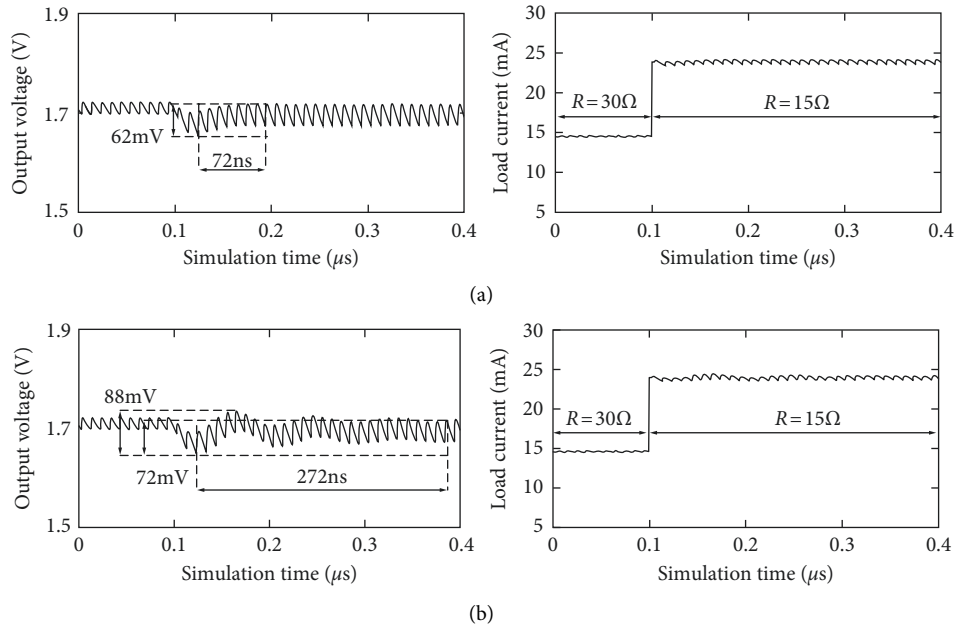

(a)

(b)

FIGURE 13: V_o and i_o of the designed boost converter with $\min(((2(M-1))/(d_1 T_s)), (2/d_1 T_s)) < (2((M-1)/M)^2/(d_1^2 T_s))$ ($V_i = 1.2$ V, $f_s = 100$ MHz, $C = 20$ nF, $L = 2$ nH, and $R = 30/15\,\Omega$) and PM = 45°. (a) Compensator based on SSA. (b) Compensator based on CA.

Figures 10–13. These figures confirm the correctness of the proposed selection strategy in Table 5.

Figure 12 presents the simulated output voltage V_o and load current i_o of the designed closed-loop controlled buck converter during a load transient, applying a Type II compensator. As indicated in Table 5, the CA method is more accurate with the condition $((2M)/(d_1 T_s(1-M))) > ((2M^2)/(d_1^2 T_s))$, and the simulated result (Figure 12) also confirms that the closed-loop controller designed with the CA method exhibits better stability and transient response than the SSA method, even though both cases have the same phase margin (PM) of 45°. On the other hand, Figure 13 shows the simulated V_o and the i_o of the closed-loop controlled boost converter during a load transient, applying also a Type II compensator. In this case, as indicated in Table 5, the SSA modeling method is more accurate with the condition $(\min((2(M-1))/(d_1 T_s)), (2/d_1 T_s)) < ((2((M-1)/M)^2)/(d_1^2 T_s))$ and the simulated result

(Figure 13) also confirms that the closed-loop controller designed with SSA method obtain a better stability and transient response. When there is a sudden change of the i_o, the boost converter with the SSA method responds faster than that with the CA method.

Unlike the conclusion made in [6], this paper shows that, in some cases, the CA method exhibits better accuracy than the SSA method. Figures 12 and 13 confirm that an accurate modeling method is critical to design the appropriate closed-loop controller of the DC-DC converter, demonstrating that the selection strategy given in Table 5 is essential and necessary in the design. The general and streamlined small signal deduction process for both modeling methods can be further applied conveniently to similar DC-DC converter topologies.

8. Conclusions

This paper presented the review, study, DCM small signal modeling deduction and simulation verification by using the improved SSA and CA methods for four DC-DC converters. This paper first proposed a general and intuitive deriving process for the improved SSA and CA modeling methods, such that the corresponding DCM small signal models for DC-DC converters can be easily determined. Then, this paper discovers that the CA can obtain higher accuracy than the improved SSA at some operating conditions, as some research studies claimed that the improved SSA can obtain the highest accuracy among all the modeling methods. Finally, this paper provided a selection strategy for a high-accuracy modeling method for various DC-DC converters operating in DCM, verified by simulations, which is necessary and beneficial in the design of a more accurate DCM closed-loop controller for DC-DC converters, achieving better stability and transient response.

Conflicts of Interest

The authors declare that there are no conflicts of interest regarding the publication of this paper.

Acknowledgments

References

[1] R. D. Middlebrook and S. Cuk, "A general unified approach to modelling switching-converter power stages," in *Proceedings of IEEE Annual Power Electronics Specialists Conference (PESC)*, pp. 18–34, Cleveland, OH, USA, 1976.

[2] R. Tymerski and V. Vorperian, "Generation, classification and analysis of switched-mode DC-to-DC converters by the use of converter cells," in *Proceedings of International Telecommunications Energy Conference*, pp. 181–195, Toronto, Canada, 1986.

[3] D. Maksimovic and S. Cuk, "A unified analysis of PWM converters in discontinuous modes," *IEEE Transactions on Power Electronics*, vol. 6, no. 3, pp. 476–490, 1991.

[4] E. Mamarelis, G. Petrone, and G. Spagnuolo, "An hybrid digital-analog sliding mode controller for photovoltaic applications," *IEEE Transactions on Industrial Informatics*, vol. 9, no. 2, pp. 1094–1103, 2013.

[5] V. Vorperian, "Simplified analysis of PWM converters using model of PWM switch. II. Discontinuous conduction mode," *IEEE Transactions on Aerospace and Electronic Systems*, vol. 26, no. 3, pp. 497–505, 1990.

[6] J. Sun, D. M. Mitchell, M. F. Greuel, P. T. Krein, and R. M. Bass, "Averaged modeling of PWM converters operating in discontinuous conduction mode," *IEEE Transactions on Power Electronics*, vol. 16, no. 4, pp. 482–492, 2001.

[7] K. Mandal, S. Banerjee, and C. Chakraborty, "A new algorithm for small-signal analysis of DC–DC converters," *IEEE Transactions on Industrial Informatics*, vol. 10, no. 1, pp. 628–636, 2014.

[8] R. H. G. Tan and M. Y. W. Teow, "A comprehensive modeling, simulation and computational implementation of buck converter using MATLAB/Simulink," in *Proceedings of IEEE Conference on Energy Conversion*, pp. 37–42, Johor Bahru, Malaysia, 2014.

[9] J. P. Torreglosa, P. García, L. M. Fernández, and F. Jurado, "Predictive control for the energy management of a fuel-cell–battery–supercapacitor tramway," *IEEE Transactions on Industrial Informatics*, vol. 10, no. 1, pp. 276–285, 2014.

[10] M. K. Kazimierczuk, *Pulse-Width Modulated DC-DC Power Converters*, Wiley, West Sussex, UK, 2008.

[11] J. Sun, D. M. Mitchell, M. F. Greuel, P. T. Krein, and R. M. Bass, "Modeling of PWM converters in discontinuous conduction mode. A reexamination," in *Proceedings of IEEE Annual Power Electronics Specialists Conference (PESC)*, pp. 615–622, Fukuoka, Japan, 1998.

[12] W. R. Liou, W. B. Lacorte, A. B. Caberos et al., "A programmable controller IC for DC/DC converter and power factor correction applications," *IEEE Transactions on Industrial Informatics*, vol. 9, no. 4, pp. 2105–2113, 2013.

[13] W. L. Zeng, C.-S. Lam, W.-M. Zheng et al., "DCM operation analysis of ky converter," *Electronics Letters*, vol. 51, no. 24, pp. 2037–2039, 2015.

[14] Y. Qiu, X. Y. Chen, C. Q. Zhong, and C. Qi, "Uniform models of PWM DC–DC converters for discontinuous conduction mode considering parasitics," *IEEE Transactions on Industrial Electronics*, vol. 61, no. 11, pp. 6071–6080, 2014.

[15] A. Davoudi, J. Jatskevich, and T. De Rybel, "Numerical state-space average-value modeling of PWM DC-DC converters operating in DCM and CCM," *IEEE Transactions on Power Electronics*, vol. 21, no. 4, pp. 1003–1012, 2006.

[16] M. U. Iftikhar, P. Lefranc, D. Sadarnac, and C. Karimi, "Theoretical and experimental investigation of averaged modeling of non-ideal PWM DC-DC converters operating in DCM," in *Proceedings of IEEE Annual Power Electronics Specialists Conference (PESC)*, pp. 2257–2263, Rhodes, Greece, 2008.

[17] R. Trinchero, I. S. Stievano, and F. G. Canavero, "Steady-state analysis of switching power converters via augmented time-invariant equivalents," *IEEE Transactions on Power Electronics*, vol. 29, no. 11, pp. 5657–5661, 2014.

[18] T. Pavlovic, T. Bjazic, and Z. Ban, "Simplified averaged models of DC-DC power converters suitable for controller design and microgrid simulation," *IEEE Transactions on Power Electronics*, vol. 28, no. 7, pp. 3266–3276, 2013.

[19] E. Van Dijk, J. N. Spruijt, D. M. O'Sullivan, and J. B. Klaassens, "PWM-switch modeling of DC-DC converters," *IEEE Transactions on Power Electronics*, vol. 10, no. 6, pp. 659–665, 1995.

[20] C. P. Basso, *Switch-Mode Power Supplies*, McGraw-Hill, New York, NY, USA, 2008.

[21] R. W. Erickson and D. Maksimovic, *Fundamentals of Power Electronics*, Kluwer Academic Publisher, Norwell, MA, USA, 2001.

[22] G. Nirgude, R. Tirumala, and N. Mohan, "A new, large-signal average model for single-switch DC-DC converters operating in both CCM and DCM," in *Proceedings of IEEE Annual Power Electronics Specialists Conference (PESC)*, vol. 3, pp. 1736–1741, Vancouver, BC, Canada, 2001.

[23] K. I. Hwu and Y. T. Yau, "KY converter and its derivatives," *IEEE Transactions on Power Electronics*, vol. 24, no. 1, pp. 128–137, 2009.